

**TABLE 2**  
Regional SUV and Regional-to-Cerebellar SUV Ratio of <sup>11</sup>C-BF-227 in Normal Subjects and AD Patients

Distribution	SUV			SUV ratio			Cohen's <i>d</i> Aged normal vs. AD
	All normal	Aged normal	AD	All normal	Aged normal	AD	
Frontal	1.13 ± 0.23	1.11 ± 0.24	1.24 ± 0.27	0.99 ± 0.04	0.99 ± 0.05	1.13 ± 0.06*	2.54
Lateral temporal	1.16 ± 0.22	1.15 ± 0.23	1.38 ± 0.30	1.03 ± 0.05	1.02 ± 0.04	1.25 ± 0.06*	4.51
Parietal	1.22 ± 0.24	1.19 ± 0.24	1.36 ± 0.30	1.08 ± 0.06	1.06 ± 0.05	1.24 ± 0.06*	3.26
Temporooccipital	1.22 ± 0.23	1.21 ± 0.24	1.35 ± 0.27	1.08 ± 0.06	1.08 ± 0.06	1.23 ± 0.09*	1.96
Occipital	1.23 ± 0.23	1.21 ± 0.24	1.32 ± 0.26	1.09 ± 0.06	1.08 ± 0.06	1.20 ± 0.07*	1.84
Anterior cingulate	1.19 ± 0.26	1.16 ± 0.26	1.27 ± 0.26	1.04 ± 0.04	1.03 ± 0.04	1.16 ± 0.06*	2.55
Posterior cingulate	1.28 ± 0.25	1.24 ± 0.25	1.38 ± 0.26	1.13 ± 0.08	1.11 ± 0.08	1.26 ± 0.04*	2.37
Medial temporal	1.33 ± 0.24	1.31 ± 0.25	1.31 ± 0.27	1.18 ± 0.07	1.17 ± 0.07	1.20 ± 0.10	0.35
Striatum	1.57 ± 0.34	1.52 ± 0.34	1.62 ± 0.34	1.38 ± 0.08	1.35 ± 0.06	1.47 ± 0.06*	2.00
Thalamus	1.78 ± 0.44	1.70 ± 0.41	1.73 ± 0.36	1.56 ± 0.12	1.51 ± 0.09	1.58 ± 0.11	0.70
Pons	1.90 ± 0.34	1.87 ± 0.34	1.91 ± 0.39	1.68 ± 0.08	1.67 ± 0.08	1.74 ± 0.09	0.82
White matter	1.64 ± 0.27	1.61 ± 0.28	1.69 ± 0.33	1.45 ± 0.11	1.44 ± 0.11	1.55 ± 0.12	0.96
Cerebellum	1.14 ± 0.23	1.13 ± 0.24	1.10 ± 0.23				

\**P* < 0.05 vs. aged normal group.

vivo imaging of amyloid. FDDNP specifically binds to both SPs and NFTs in AD brain sections (19). After intravenous injection of FDDNP, greater accumulation was observed in SP- and NFT-rich areas of the human brain (20). Thioflavin-T derivatives without any positive charge also show high permeability of the BBB. One of these compounds, PIB, was applied in a human PET study and enabled successful differentiation between AD patients and healthy normal individuals (5). Another amyloid-imaging agent, SB-13, was also applied in a human PET study and exhibited binding properties similar to those of PIB (21). Several iodinated agents, IMPY and I-stilbene, have also been explored for use as SPECT probes (22). Although validation remains necessary to determine whether retention of these agents in the neocortex truly reflects the level of amyloid deposition, such findings suggest the potential usefulness of this technique for early diagnosis of AD.

[AQ9]

The results of the in vitro binding experiment indicate that binding of BF-227 reflects the amount of Aβ fibril deposition. In neuropathologic staining of AD brain sections, the fluorescence intensity of BF-227 is highest in the core region of mature amyloid deposits, which contain dense fibrils of Aβ. Conversely, diffuse plaques containing fewer Aβ fibrils are faintly stained by BF-227. SPs in the cerebellum are predominantly of the nonfibrillar type (23,24), and BF-227 only faintly stained diffuse amyloid plaques in the cerebellum. Thus, the absence of <sup>11</sup>C-BF-227 accumulation in the cerebellum of AD patients suggests the binding preference of this compound for fibrillar Aβ. This finding also indicates that the cerebellum is suitable as a reference region in the quantitative analysis of <sup>11</sup>C-BF-227 PET data.

PIB is currently the most successful of several amyloid-imaging agents. A clinical PET study in AD patients showed higher uptake of PIB in cortical areas and striatum, particularly the frontal and parietal cortices (5–7). In contrast, the

current study demonstrated higher cortical retention of <sup>11</sup>C-BF-227 in the temporoparietal–occipital region rather than that in the frontal cortex and the striatum in AD patients. Both agents are considered to preferentially bind to the β-sheet structure of Aβ fibrils. What other factors could

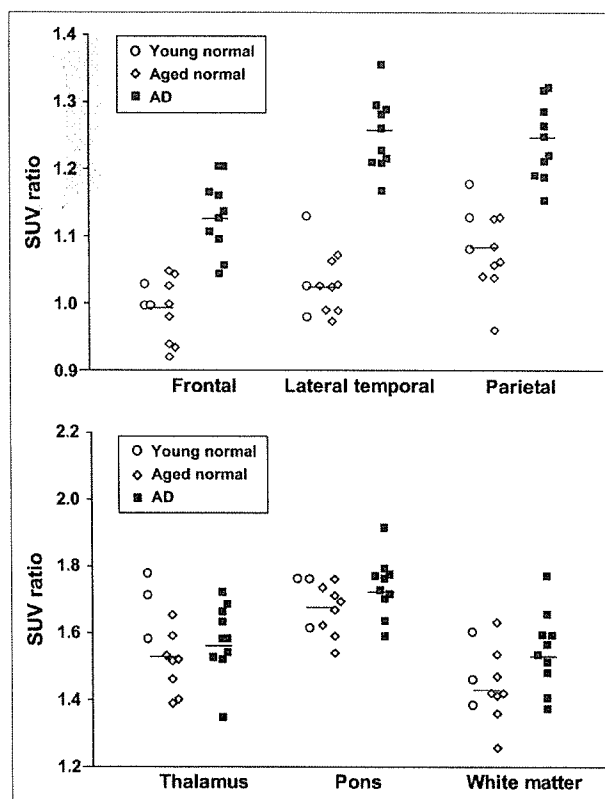


**FIGURE 6.** ROI/cerebellar SUV ratio in young normal subjects (○), aged normal subjects (◇), and AD patients (■). Vertical bar represents average SUV ratio in all normal subjects (*n* = 11) and AD patients (*n* = 10).

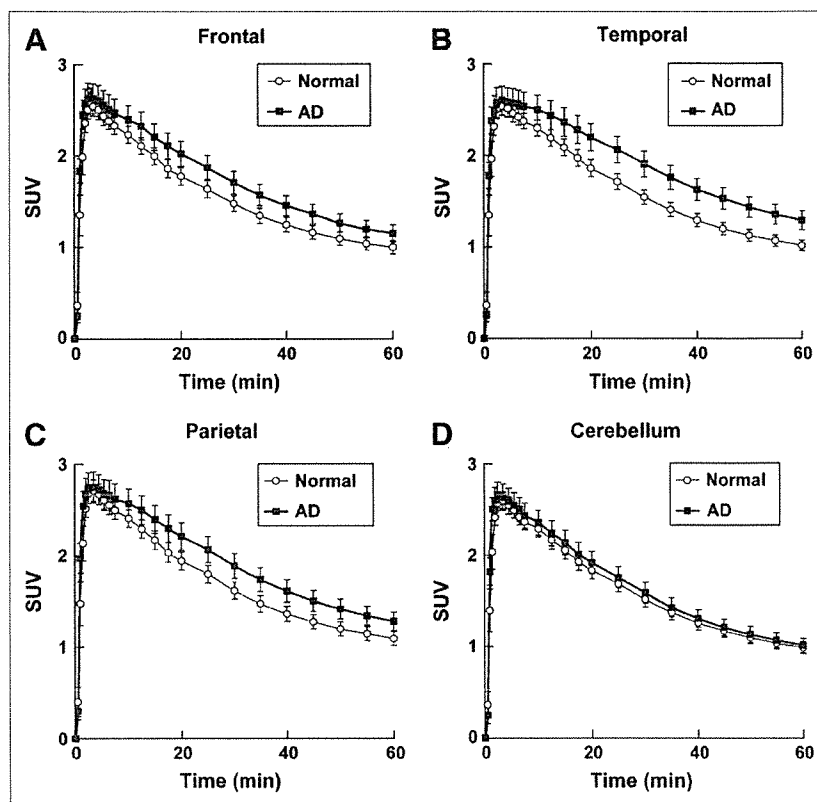


**FIGURE 4.** Time-activity data for  $^{11}\text{C}$ -BF-227 PET in humans. SUV time-activity curves of  $^{11}\text{C}$ -BF-227 in frontal cortex (A), temporal cortex (B), parietal cortex (C), and cerebellum (D) are shown. Each point represents mean  $\pm$  SEM of data from 7 AD patients and 7 normal control subjects.

pons, and white matter was nearly identical in AD patients and normal subjects. The effect size value between AD patients and aged normal subjects was highest in the lateral temporal cortex, which was followed by the parietal, anterior cingulate, and frontal cortices, and was lowest in the medial temporal, thalamus, and pons (Table 2). No significant difference was observed in any brain regions between young normal and aged normal subjects, although aged individuals tended to exhibit a higher SUV ratio in the frontal cortex than young individuals (data not shown).

#### Voxel-by-Voxel Analysis of $^{11}\text{C}$ -BF-227 PET Images

In comparison with aged normal subjects, AD patients showed significantly higher uptake of  $^{11}\text{C}$ -BF-227 in the bilateral temporoparietal region ( $[50, -56, 6]$ ,  $Z = 5.41$ ,  $k = 22,823$ ), including the posterior cingulate cortex and the left middle frontal gyrus ( $[-26, 24, 40]$ ,  $Z = 3.79$ ,  $k = 1,401$ ) in SPM analysis (Fig. 7). These areas corresponded well with the region containing a high density of neuritic plaques. In contrast, no significant region was detected showing lower uptake of  $^{11}\text{C}$ -BF-227 in the AD group than that in the normal group.

#### DISCUSSION

BF-227 was designed to improve BBB penetration and clearance from normal brain tissue, without deteriorating the high binding affinity of benzoxazole derivatives to  $\text{A}\beta$ .

Several lipophilic compounds have been reported as potential amyloid imaging probes. 2-(1-{6-[(2-Fluoroethyl)(methyl)amino]-2-naphthyl}ethylidene)malononitrile (FDDNP) was introduced as the first BBB-permeable compound for in

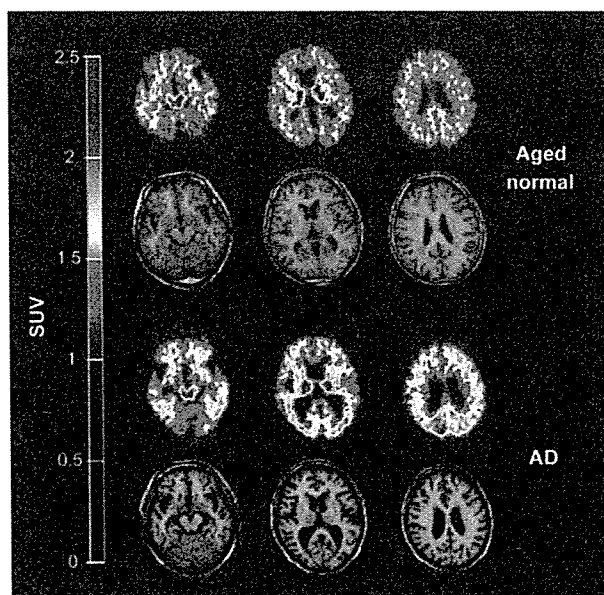


**FIGURE 5.** Mean SUV images between 20 and 40 min after injection of  $^{11}\text{C}$ -BF-227 in aged normal subject (top, 70-y-old woman) and AD patient (bottom, 68-y-old woman). Coregistered MR images are shown below PET images.

4/C

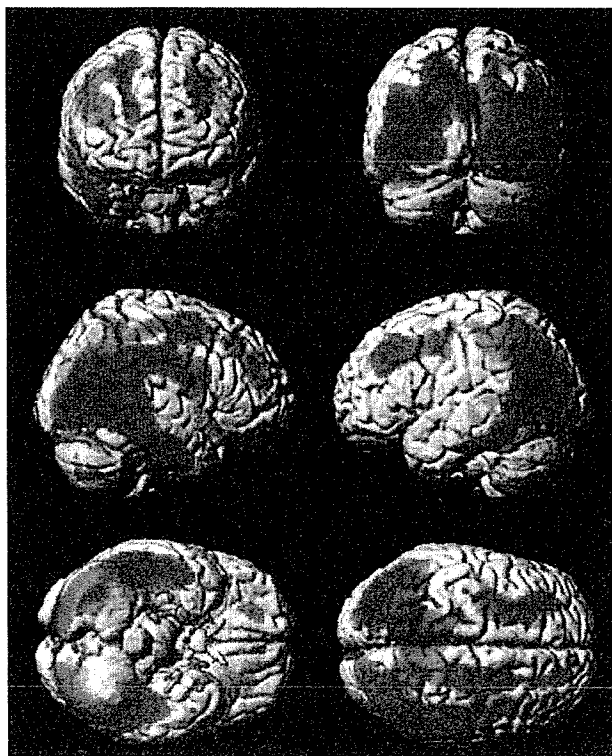


**FIGURE 7.** Brain regions show significantly elevated SUVs in AD patients (left) compared with aged normal subjects (right) [AQ14] ( $P < 0.001$ , uncorrected for multiple comparisons).

have caused the difference of tracer distribution between previous PIB studies and the current BF-227 study? Generally, substantial individual variations exist in the amount and spatial distribution of amyloid deposition in AD. Thus, the discrepancy might be partially attributable to a difference in sample populations between studies. To settle this issue, a direct comparison study between PIB and BF-227 should be conducted using the same sample populations. SP is a heterogeneous class of protein aggregates with a  $\beta$ -pleated structure. Compact plaques consist of a dense central core of amyloid fibrils, and noncompact plaques contain less fibrillar  $A\beta$  (25). Therefore, it would be expected that the lower-affinity compound would tend to detect only SPs with dense  $A\beta$  fibrils and that the higher-affinity compound could bind SPs with both dense and moderately fibrillar  $A\beta$ . In AD patients, the difference between cortical and cerebellar SUV in  $^{11}\text{C}$ -BF-227 PET was less than that in PIB PET (5–7), suggesting that the *in vivo* binding affinity of BF-227 to  $A\beta$  deposits is relatively lower than that of PIB. If so, BF-227 binds more preferentially to dense amyloid deposits than PIB. Previous neuropathologic studies have indicated that neuritic plaque densities are highest in the neocortex, especially the temporoparieto-occipital region, and lowest in the cerebellum (18,26). Data from SPM analysis are consistent with the postmortem distribution of neuritic plaque deposition in AD patients. Therefore, the difference in cortical distribution between

BF-227 and PIB might be due to the difference in binding affinity to  $A\beta$  fibrils. A PET probe binding selectively to neuritic plaques would be less subject to  $A\beta$  pathology in the normal aging process. Thus, use of  $^{11}\text{C}$ -BF-227 PET will allow accurate diagnosis of AD and might reduce false-positive findings in normal individuals.  $^{11}\text{C}$ -BF-227 PET might also be useful for tracking the progression of fibrillar  $A\beta$  deposition in AD patients. Longitudinal PET investigation of AD patients will elucidate the utility of this imaging technique for monitoring disease progression in AD.

NFTs stained faintly with BF-227, suggesting that BF-227 has a relatively lower binding affinity to NFTs than SPs, which might explain the lack of significant difference in the medial temporal SUV of  $^{11}\text{C}$ -BF-227. However, 3 AD patients (AD 1, AD 2, and AD 3 in Table 1) exhibiting high BF-227 accumulation in the cerebral cortex showed higher accumulation in the medial temporal cortex than the other AD patients. This finding might reflect the increasing deposition of amyloid plaques in the medial temporal cortex of the 3 AD patients. Thalamic and white matter accumulation of  $^{11}\text{C}$ -BF-227 was considerable in both AD patients and normal subjects. Retention levels of  $^{11}\text{C}$ -BF-227 in these regions were nearly identical between normal and AD groups. Therefore, these retentions are not likely to reflect AD-specific pathology. BF-227 retention in these sites may be related to the many myelinated fibers present in these structures, because myelin basic protein—one of the major myelin proteins in the brain—partially shares the same structure with amyloid fibrils, and some  $\beta$ -sheet binding agents bind to this protein (27–29). Clearance of  $^{11}\text{C}$ -BF-227 from normal brain tissue was slower than that of PIB. This might be caused by the difference in lipophilicity between BF-227 and PIB. BF-227 ( $\log P = 1.75$ ) is more lipophilic than PIB ( $\log P = 1.20$ ) (30) because, unlike PIB, BF-227 does not have a hydroxy group. Compounds [AQ10] that are too lipophilic will be bound by plasma protein and undergo rapid metabolism by the liver; therefore, they may display reduced brain uptake. Moreover, lipophilic radioligands display a higher nonspecific binding in the brain and, thus, high nonspecific binding may explain the moderate difference in BF-227 uptake between AD patients and normal control subjects. In general, the introduction of a hydroxy group into a molecule changes the partition coefficient toward more hydrophilicity. Therefore, the hydroxylated BF-227 derivative would be expected to show faster clearance from normal brain tissue and a better signal-to-noise ratio than BF-227. We are now implementing the optimizing process to reduce white matter retention and plan to apply the optimized compound to the candidate for an  $^{18}\text{F}$ -labeled PET probe.

## CONCLUSION

The present study demonstrated that the benzoxazole derivative BF-227 displays high binding affinity to amyloid

plaques and high BBB permeability. The current clinical trial indicated that BF-227 has adequate safety to be used clinically as a PET probe. <sup>11</sup>C-BF-227 PET demonstrated significant retention of this agent in sites with a preference for the deposition of dense amyloid plaques and distinctly differentiated between AD patients and normal individuals. Collectively, these findings suggest that <sup>11</sup>C-BF-227 is useful for early diagnosis of AD.

#### ACKNOWLEDGMENTS

This study was supported by the Program for the Promotion of Fundamental Studies in Health Science by the National Institute of Biomedical Innovation, the Industrial Technology Research Grant Program in 2004 from the New Energy and Industrial Technology Development Organization of Japan, Health and Labour Sciences Research Grants for Translational Research from the Ministry of Health, Astrazeneca Research Grant 2004, and the Novartis Foundation for Gerontological Research. We appreciate the technical assistance of Dr. S. Watanuki and Dr. Y. Ishikawa in the clinical PET studies and Dr. M. Kato in the imaging analysis. We also thank to Dr. H. Akatsu and Dr. T.

[AQ11] Yamamoto for supplying brain samples.

#### REFERENCES

- Morris JH, Nagy Z. Alzheimer's disease. In: Esiri MM, Lee VM, Trojanowski JQ, eds. *The Neuropathology of Dementia*. 2nd ed. Cambridge, U.K.: Cambridge University Press; 2004:161–206.
- Goldman WP, Price JL, Storandt M, et al. Absence of cognitive impairment or decline in preclinical Alzheimer's disease. *Neurology*. 2001;56:361–367.
- Price JL, Morris JC. Tangles and plaques in nondemented aging and "preclinical" Alzheimer's disease. *Ann Neurol*. 1999;45:358–368.
- Aisen PS. The development of anti-amyloid therapy for Alzheimer's disease: from secretase modulators to polymerisation inhibitors. *CNS Drugs*. 2005;19:989–996.
- Klunk WE, Engler H, Nordberg A, et al. Imaging brain amyloid in Alzheimer's disease with Pittsburgh Compound-B. *Ann Neurol*. 2004;55:306–319.
- Price JC, Klunk WE, Lopresti BJ, et al. Kinetic modeling of amyloid binding in humans using PET imaging and Pittsburgh Compound-B. *J Cereb Blood Flow Metab*. 2005;25:1528–1547.
- Lopresti BJ, Klunk WE, Mathis CA, et al. Simplified quantification of Pittsburgh Compound B amyloid imaging PET studies: a comparative analysis. *J Nucl Med*. 2005;46:1959–1972.
- Price JL. Diagnostic criteria for Alzheimer's disease. *Neurobiol Aging*. 1997;18(suppl):S67–S70.
- Wang J, Dickson DW, Trojanowski JQ, Lee VM. The levels of soluble versus insoluble brain A $\beta$  distinguish Alzheimer's disease from normal and pathologic aging. *Exp Neurol*. 1999;158:328–337.
- Okamura N, Suemoto T, Shimadzu H, et al. Styrylbenzoxazole derivatives for in vivo imaging of amyloid plaques in the brain. *J Neurosci*. 2004;24:2535–2541.
- Okamura N, Suemoto T, Shiomitsu T, et al. A novel imaging probe for in vivo detection of neuritic and diffuse amyloid plaques in the brain. *J Mol Neurosci*. 2004;24:247–255.
- Shimadzu H, Suemoto T, Suzuki M, et al. Novel probes for imaging amyloid- $\beta$ : F-18 and C-11 labeling of 2-(4-aminostyryl)benzoxazole derivatives. *J Labelled Compds Radiopharm*. 2004;47:181–190.
- Jewett DM. A simple synthesis of [<sup>11</sup>C]methyl triflate. *Appl Radiat Isot*. 1992;43:1383–1385.
- Iwata R, Pascale C, Bogner A, Miyake Y, Yanai K, Ido T. A simple loop method for the automated preparation of [<sup>11</sup>C]raclopride from [<sup>11</sup>C]methyl triflate. *Appl Radiat Isot*. 2001;55:17–22.
- Holcomb L, Gordon MN, McGowan E, et al. Accelerated Alzheimer-type phenotype in transgenic mice carrying both mutant amyloid precursor protein and presenilin 1 transgenes. *Nat Med*. 1998;4:97–100.
- Friston KJ, Holmes AP, Worsley KJ, Poline JP, Frith CD, Frackowiack RSJ. Statistical parametric maps in functional imaging: a general linear approach. *Hum Brain Mapp*. 1995;2:189–210.
- Higuchi M, Tashiro M, Arai H, et al. Glucose hypometabolism and neuropathological correlates in brains of dementia with Lewy bodies. *Exp Neurol*. 2000;162:247–256.
- Arnold SE, Hyman BT, Flory J, Damasio AR, Van Hoesen GW. The topographical and neuroanatomical distribution of neurofibrillary tangles and neuritic plaques in the cerebral cortex of patients with Alzheimer's disease. *Cereb Cortex*. 1991;1:103–116.
- Agdeppa ED, Kepe V, Liu J, et al. Binding characteristics of radiofluorinated 6-dialkylamino-2-naphthylethylidene derivatives as positron emission tomography imaging probes for beta-amyloid plaques in Alzheimer's disease. *J Neurosci*. 2001;21:RC189.
- Shoghi-Jadid K, Small GW, Agdeppa ED, et al. Localization of neurofibrillary tangles and beta-amyloid plaques in the brains of living patients with Alzheimer disease. *Am J Geriatr Psychiatry*. 2002;10:24–35.
- Verhoeff NP, Wilson AA, Takeshita S, et al. In-vivo imaging of Alzheimer disease beta-amyloid with [<sup>11</sup>C]SB-13 PET. *Am J Geriatr Psychiatry*. 2004;12:584–595.
- Kung HF, Kung MP, Zhuang ZP, et al. Iodinated tracers for imaging amyloid plaques in the brain. *Mol Imaging Biol*. 2003;5:418–426.
- Yamaguchi H, Hirai S, Morimatsu M, Shoji M, Nakazato Y. Diffuse type of senile plaques in the cerebellum of Alzheimer-type dementia demonstrated by beta protein immunostain. *Acta Neuropathol (Berl)*. 1989;77:314–319.
- Yamazaki T, Yamaguchi H, Nakazato Y, Ishiguro K, Kawarabayashi T, Hirai S. Ultrastructural characterization of cerebellar diffuse plaques in Alzheimer's disease. *J Neuropathol Exp Neurol*. 1992;51:281–286.
- Dickson DW. The pathogenesis of senile plaques. *J Neuropathol Exp Neurol*. 1997;56:321–339.
- Joachim CL, Morris JH, Selkoe DJ. Diffuse senile plaques occur commonly in the cerebellum in Alzheimer's disease. *Am J Pathol*. 1989;135:309–319.
- Bjelke B, Seiger A. Morphological distribution of MBP-like immunoreactivity in the brain during development. *Int J Dev Neurosci*. 1989;7:145–164.
- Ridsdale RA, Beniac DR, Tompkins TA, Moscarello MA, Harauz G. Three-dimensional structure of myelin basic protein. II. Molecular modeling and considerations of predicted structures in multiple sclerosis. *J Biol Chem*. 1997;272:4269–4275.
- Stankoff B, Wang Y, Bottlaender M, et al. Imaging of CNS myelin by positron-emission tomography. *Proc Natl Acad Sci U S A*. 2006;103:9304–9309.
- Mathis CA, Wang Y, Holt DP, Huang GF, Debnath ML, Klunk WE. Synthesis and evaluation of <sup>11</sup>C-labeled 6-substituted 2-arylbenzothiazoles as amyloid imaging agents. *J Med Chem*. 2003;46:2740–2754.

[AQ13]

[AQ12]



特集 ■ 分子イメージング

## 分子イメージング総論

An Introduction and General Remarks for Molecular Imaging

福田 寛<sup>1)</sup> 岡村 信行<sup>2)</sup>Hiroshi Fukuda<sup>1)</sup>, Nobuyuki Okamura<sup>2)</sup>

## Abstract

Molecular imaging is a visualization of quantity and dynamics of molecules to understand the process of gene regulation and physiological function of the proteins in living tissue or cells. Examples of the research include the development and application of fluorescent proteins, quantum dots, nanoparticles for optical imaging, micro bubbles for ultrasound, ferromagnetic compounds for MRI and radiopharmaceuticals for positron emission tomography (PET). PET is most promising in this field, because of its high sensitivity of the measurement and easy applicability to humans. In this general remark, the topics will be concentrated on molecular imaging with PET for the diagnosis of Alzheimer's disease (AD) in early stage.

<sup>11</sup>C-MP4P (N-methylpiperidyl-4-propionate), is a probe for the measurement of acetylcholine esterase (AChE) activity in the human brain by PET. The AChE activities (k3) in early onset AD measured with PET was low in hippocampus, amygdale and wide spread neocortex including parietal and temporal cortex compared to those in age-matched control. The results indicated that the decrease of AChE activities is preceded by the decrease of blood flow. One of the topics in this research field is an imaging of aggregated amyloid A $\beta$  in the AD brain. Kudo et al, screened more than 2,600 compounds and found several good probes for amyloid A $\beta$  imaging, including BF-168 and BF-227. Okamura demonstrated that BF-168 specifically bind to the amyloid plaques in the brain of a transgenic mouse (PS1/APPsw). Furumoto et al successfully labeled BF-227 with C-11, and clinical PET studies using <sup>11</sup>C-BF-227 is now ongoing at Tohoku University. Preliminary clinical study revealed that the compound accumulated in the tempo-parietal region of the brain in AD patient, although non-specific accumulation in the thalamus, basal ganglia and white matter was observed. The goal of this project is to detect AD at pre-clinical stage.

Key words : molecular imaging with PET, Alzheimer's disease, acetylcholine esterase, amyloid A $\beta$  imaging

## はじめに

分子イメージングという言葉は「生体内の分子の挙動を可視化」する技術、およびその応用研究を意味するが、実際にはかなり幅広い意味で用いられており、厳密な定義はないのが実情である。標識化合物を利用して生体の血流、代謝、受容体結合など、生体内分子の挙動を画像化する PET (positron emission tomography), あるいは SPECT (single photon emission computed tomogra-

phy) は、すべて広い意味での分子イメージング法といえる。一方、基礎生命科学、分子生物学の飛躍的な発展により遺伝子の発現、すなわちゲノムに始まる転写、翻訳、蛋白合成、生理機能発現までの一連の生命現象の流れを解明することが現代科学の本流となっており、これらの過程における遺伝子や蛋白など生体分子の量や機能、挙動を画像化する試みがなされている。後者が本来の意味での分子イメージングであろう。

米国においては、国を挙げてこの分野の研究を推進することを旨として、2000年に国立生体イメージング・生

1) 東北大学加齢医学研究所機能画像医学研究分野 (〒980-8575 仙台市青葉区星陵町 4-1) Department of Nuclear Medicine and Radiology, Institute of Development, Aging and Cancer, Tohoku University, 4-1 Seiryō-machi, Aoba-ku, Sendai 980-8575, Japan

2) 東北大学大学院医学系研究科機能薬理学分野 Department of Pharmacology, Graduate School of Medicine, Tohoku University

体工学研究所 (NIBIB: National Institute of Biomedical Imaging and Bioengineering) が設立された。この研究所の設立目的には「物理学, 化学, 数学, 計算機科学, 工学に関する諸原理を統合して, 生物学, 医学, 行動学および健康について研究をすすめて基礎的学問を発展させ, 分子から器官にいたる知識を生み出し, 最終的には病気を予防, 診断, 治療し健康増進を行う」ことが掲げられている。このプロジェクトではさまざまな研究アプローチの中でも, イメージングが特に強調されている。また, 米国の国立癌研究所 (NCI: National Cancer Institute) では, 全米に5カ所, 生体分子細胞イメージングセンター (ICMIC: In Vivo Cellular and Molecular Imaging Center) を設立して, この分野の研究を推進している。

一方, わが国でも2005年度に, 放射線医学総合研究所および理化学研究所を中心として分子イメージング・プロジェクトがスタートした。放射線医学総合研究所では, PET 疾患診断研究拠点担当として, (1)次世代分子イメージング技術の研究開発, (2)精神・神経疾患のイメージング研究, (3)腫瘍イメージング研究を3本柱として研究を推進している。また, 東北大学も研究推進および人材育成の点で, 放医研と連携してプロジェクトを進めている。理化学研究所では, 創薬候補物質探索拠点担当として, PET を用いる分子イメージング用分子プローブの設計・機能評価・動態評価応用を通じて, 創薬プロセスの効率化・短縮を目指している。

さらに, このような分子イメージング研究の機運をとらえて2006年5月に「日本分子イメージング学会」が発足した(藤林会長, 福井大学)。米国に遅れること約5年であるが, ようやくわが国においても分子イメージング研究の幕が開いたといえる。分子イメージングは, 分子の挙動から見た生命現象の解明に大きな貢献が期待されているが, その最終的な目標は疾患の早期診断, あるいは臨床的な症状はないが疾患リスクの高い者の診断など, より予防医学的観点から, 感度と特異度の高いプローブを開発することである。

## I. 分子イメージングの方法

分子イメージングを行うには, なんらかの方法で標識した分子プローブが必要である。用いる標識法, マーカーの種類, 測定・画像化原理によって大別すると, 蛍光色素あるいは蛍光人工粒子を用いる光イメージング法(蛍光イメージング), 放射性標識化合物を用いるPET法, 磁性化合物を用いるMRI法がある。本稿では, PETに

よるイメージングを中心に述べ, それ以外の方法については簡単に記すことにする。

### 1. PETによる分子イメージング

PETは $^{18}\text{F}$ (半減期110分),  $^{11}\text{C}$ (半減期20分),  $^{15}\text{O}$ (半減期2分)などの短寿命のポジトロン(陽電子)を放出する核種で標識した化合物を用いる, 核医学画像診断法の1つである。ヒトに応用できる分子イメージング技術であること, 多様な標識プローブの開発が可能であることから, 疾患病態解明, 診断・治療法の開発, 創薬における分子イメージング研究の手段として最も期待されている。

脳機能の画像化に関しては, PET研究の初期には血流( $\text{C}^{15}\text{O}_2$ ,  $\text{H}_2^{15}\text{O}$ ), 酸素代謝( $^{15}\text{O}_2$ ), ブドウ糖代謝( $^{18}\text{F}$ -フルオロデオキシグルコース)の測定が主であった。これらからの分子イメージングの方向性では, より特異的な分子挙動の画像化が求められている。このような方向性の試みとしては, 神経伝達物質の合成・放出・受容体との結合・分解・再吸収に関する情報の画像化, 遺伝子導入された遺伝子の発現情報の画像化, 標識 Anti-sense nucleotide を用いた遺伝子翻訳情報画像化<sup>1)</sup>, 標識 aptamer を用いる分子構造特異的情報の画像化<sup>2)</sup> などがある。ここでは, アルツハイマー病(AD)の病態解明, 早期診断を目標とした研究を例に挙げて解説することにする。

#### 1) ADの分子イメージングー脳内アセチルコリンエステラーゼ活性の画像化

ADの脳画像所見としては, 両側の頭頂葉, 側頭葉連合野の脳血流, ブドウ糖代謝が低下することが報告されてきた。Minoshimaら<sup>3)</sup>は, 解剖学標準化による画像統計解析を疾患診断に応用することにより, 健常者脳血流データベースの平均値と比べて有意に血流が低下(上昇)している部位を, 画素単位で抽出する方法を開発した。この方法を用いて非常に早期のADにおいて, 後部帯状回のブドウ糖代謝が低下することを報告している。

一方, ADでは大脳皮質あるいは海馬でコリン作動性神経の脱落が古くから報告されている。このことに着目したIrie(放射線医学総合研究所)ら<sup>4,5)</sup>は, “脳内アセチルコリン分解酵素活性を測定する”目的で,  $^{11}\text{C}$ -MP4P(N-methylpiperidyl-4-propionate)を世界に先駆けて開発した。この化合物はアセチルコリンの類似化合物で, その高い脂溶性のために血流に依存して脳内に取り込まれる。次いでアセチルコリンエステラーゼ(AchE)により加水分解されて, 脂溶性が低下して脳外への逆透過が

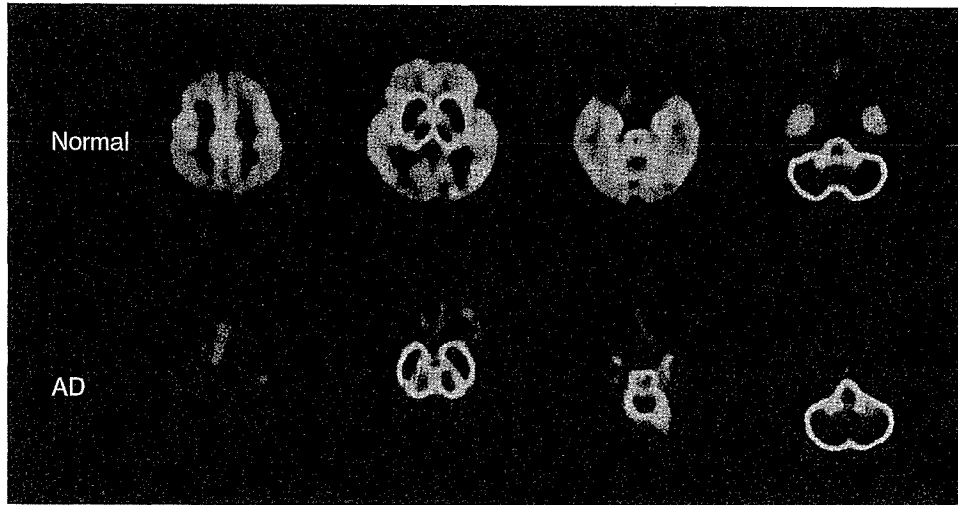


Fig. 1  $^{11}\text{C}$ -MP4P による健常高齢者および AD 患者の PET 像  
〔篠遠 仁博士 (旭神経内科病院) のご提供による。〕

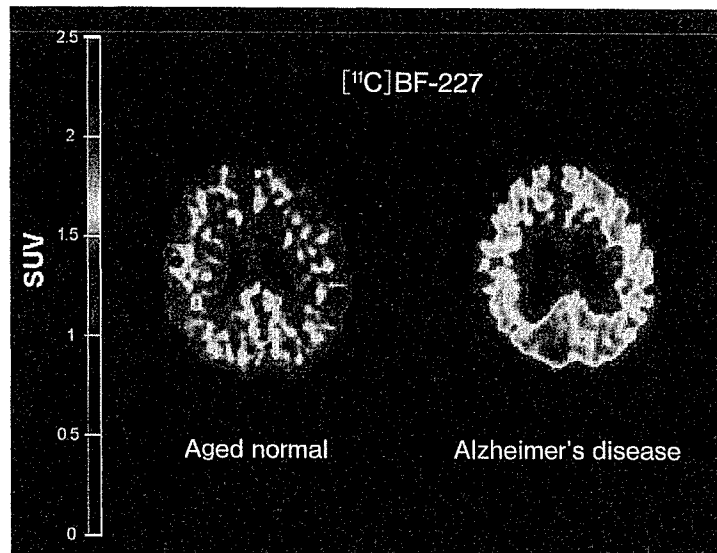


Fig. 2  $^{11}\text{C}$ -BF-227 による健常人(左)とアルツハイマー病患者(右)の PET 像

interaction) 方式の検出器を用いた次世代 PET の開発が行われており、人体用頭部専用試作機が完成している<sup>12)</sup>。通常の PET 装置では、感度を向上させるために光子入射方向に細長い結晶を配置している。このため、斜め方向から入射した光子に対して、位置分解能が著しく劣化するという欠点を持っており、視野の中心部に比べて周辺部での分解能が劣化する。DOI 方式では、深さ方向に複数の結晶を重ねてあり、どの深さで光子を検出したか弁別できる方式で、斜め方向から入射した光子は表層にある結晶とは相互作用せず、深い位置にある結晶に入射することになる。この方式により視野全体で中心

部と同じ分解能を得ることができる。

また、東北大学石井らは、半導体検出器 (CdTe) を用いた PET の開発を行っている。半導体サイズを小さくでき、効率的に集積できること、エネルギー分解能が良いことなどの特性を生かして、分解脳 1 mm 程度の PET 装置の開発を目指している。現在、動物用の試作器を制作して開発を進めている。

## 2. PET 以外の分子イメージング法

これまで GFP (green fluorescent protein) 発現遺伝子をレポーター遺伝子として組み込むことによる目的遺伝

子発現の可視化, 蛍光プローブを組み込んだ1分子イメージングによる分子挙動のダイナミクス解析など, 光イメージングは分子生物学の発展に大きく貢献してきた。この分野への期待は大きく, 現在, 米国 NIH (National Institutes of Health) では分子イメージングに関する大型研究資金が多数採択されている。人体応用を目指したプローブとしては, MR イメージング用ナノカプセル,  $MFe_2O_4$  付加ポリマーミセルによる MRI 用プローブ, 蛍光セラミックナノプローブ, 超音波用プローブ, 遺伝子レポータープローブなどの開発などがある。また, 細胞イメージング用としては, 金属ナノクラスターによる Quantum dot による1分子イメージング, 新規光イメージング用プローブのライブラリーによる網羅的探索などがある。

この分野では, 光学検出系装置の開発も重要で, さらに空間分解能および時間分解能が高い装置が求められている。理化学研究所のグループは, ナノメートルサイズの金属円柱で作成した新型レンズにより, 光の波長の限界を超えた分解能を持つ顕微鏡の開発に成功している<sup>13)</sup>。

## 最 後 に

PET を用いた AD の研究を例として, 分子イメージングの概要を述べた。PET は測定感度が他の方法に比べて高いこと, ヒトに応用できるイメージング法であることから, この分野の中心的方法論として今後もその重要性・優位性は変わらないと筆者は考えている。しかし, 光イメージング, MRI, 超音波などのための分子プローブや biomarker の開発に, 米国では集中的に研究予算が投下されており, 大きな発展が予想される。

## 謝辞

本稿で示した PET による  $\beta$  アミロイドイメージングは, 工藤幸司, 古本祥三 (東北大学先進医工学研究機構), 荒井啓行, 谷内一彦 (同医学研究科), 岩田 錬, 田代 学 (同サイクロトロンラジオアイソトープセンター) 博士らによる, 東北大学分子イメージングプロジェクトの成果である。

## 文 献

- 1) de Vries EFJ, Vroegh J, Dijkstra G, Moshage H, Elsinga PH, et al: Synthesis and evaluation of a fluorine-18 labeled antisense oligonucleotide as a potential PET tracer for iNOS mRNA expression. *Nucl Med Biol* 31: 605-612, 2004
- 2) Hicke BJ, Stephens AW, Gould TY, Chang YF, Lynott CK, et al: Tumor targeting by an aptamer. *J Nucl Med* 47: 668-678, 2006
- 3) Minoshima S, Giordani B, Berent S, Frey KA, Foster NL, et al: Metabolic reduction in the posterior cingulate cortex in very early Alzheimer's disease. *Ann Neurol* 42: 85-94, 1997
- 4) Irie T, Fukushi K, Akimoto Y, Tamagami H, Nozaki T: Design and evaluation of radioactive acetylcholine analogs for mapping brain acetylcholinesterase (AChE) *in vivo*. *Nucl Med Biol* 21: 801-808, 1994
- 5) Irie T, Fukushi K, Namba H, Iyo M, Tamagami H, et al: Brain acetylcholinesterase activity: Validation of a PET tracer in a rat model of Alzheimer's disease. *J Nucl Med* 37: 649-655, 1996
- 6) Iyo M, Namba H, Fukushi K, Shinotoh H, Nagatsuka S, et al: Measurement of acetylcholinesterase by positron emission tomography in the brain of healthy controls and patients with Alzheimer's disease. *Lancet* 349: 1805-1809, 1997
- 7) Shinotoh H, Namba H, Fukushi K, Nagatsuka S, Tanaka N, et al: Progressive loss of cortical acetylcholinesterase activity in association with cognitive decline in Alzheimer's disease: A positron emission tomography study. *Ann Neurol* 48: 194-200, 2000
- 8) Funaki Y, Kato M, Iwara R, Sakurai E, Tashiro M, et al: Evaluation of the binding characteristics of [5-<sup>14</sup>C-methoxy] Donepezil in the rat brain for *in vivo* visualization of acetylcholinesterase. *J Pharmacol Sci* 91: 105-112, 2003
- 9) 工藤幸司: 痴呆症の画像診断のためのプローブの開発研究, 医薬品副作用被害救済・研究振興調査機構研究支援事業「痴呆疾患・治療薬開発のための基盤的研究」, 株式会社ピーエフ研究所, pp239-271, 2004年6月15日
- 10) Okamura N, Suemoto T, Shimadzu H, Suzuki M, Shimadzu H, et al: Styrylbenzoxazole derivatives for *in vivo* imaging of amyloid plaques in the brain. *J Neurosci* 24: 2535-2541, 2004
- 11) Klunk WE, Engler H, Nordberg A, Wang Y, Blomqvist G, et al: Imaging of brain amyloid in Alzheimer's disease with Pittsburgh Compound-B. *Ann Neurol* 55: 306-319, 2004
- 12) 棚田修二, 村山秀雄(編): 平成17年度次世代PET装置開発研究報告書, 2006年, 3月.
- 13) Ono A, Kato J, Kawata S: Subwavelength optical imaging through a metallic nanorod array. *Phys Rev Lett* 95: 267-407, 2005



## 分子イメージング

工藤幸司

Molecular imaging

$A\beta$  と標識プローブ結合を *in vivo* で画像化し、診断しようとするのがアミロイドイメージングである。すでいくつかのプローブの探索的臨床試験が実施されており、AD の早期、鑑別、発症前診断などを可能にすると考えられている。

## はじめに

AD においては患者を取り巻く家族、または臨床家がこの疾患特有の臨床症状に気づいたときには、それぞれ  $A\beta$  および過剰リン酸化タウ蛋白を主構成成分とする老人斑および神経原線維変化などの病理像はもはや取り返しのつかないほど進行していることが知られている。すなわち、現状の AD 診断を癌のそれに例えるなら、末期状態に達した時点でしか検出されていないことになる。近年、一部 AD の前駆状態と考えられている MCI においても病理学的にはすでに立派な AD 状態であることが明らかにされていることから、AD はもの忘れ症状が発現するかなり以前からその病理像がスタートしていることになる。これらの事実は AD の臨床像と病理像、言い換えると clinical AD と pathological AD との間には大きな乖離が存在することを示唆している。

本項で紹介する  $A\beta$  分子を画像化するアミロイドイメージングは、AD の病理像としての  $\beta$  シート構造をとった  $A\beta$  を追跡することから、診断原理的に早期、鑑別、さらに発症前診断をも可能とすると考えられている。

それでは、アミロイドイメージングとはいかなるストラテジーに基づくかについて解説すると概念は以下の通りである。

- ①AD の病理学的主徴の1つ、老人斑のほとんどは  $\beta$  シート構造をとった  $A\beta$  によって形成されている。
- ②同シート構造をとった  $A\beta$  に特異的選択的に結合し、かつ容易に血液-脳関門を透過する低分子有機化合物を見出す。
- ③この化合物を PET または SPECT で扱うことが可能な核種で標識する。
- ④これをプローブとして生体に静脈内投与する。
- ⑤プローブは血液-脳関門を越えて脳内の老人斑を形成している  $A\beta$  に結合する。一定時間後には非結合プローブは洗い流され、 $A\beta$  に結合したプローブのみが脳内に残る。
- ⑥これを PET または SPECT を用い、イメージング画像として取り込み、 $\beta$  シート構造をとった脳内  $A\beta$  (=老人斑)蓄積量の定量およびその空間的分布から AD を診断する。

## AD 診断用プローブ

アミロイドイメージングを具体化させる最も高いハードルは  $\beta$  シート構造をとった  $A\beta$  に特異的選択的に結合し、かつ血液-脳関門を容易に透過し、さらに標的以外からは速やかにクリアランスされるなどの優れた特性を有するプローブを見出すことにある。これまで多くのプローブ候補化合物が報告されてきたが、これらの中で [ $^{18}\text{F}$ ] FDDNP<sup>1)</sup>、[ $^{11}\text{C}$ ] PIB<sup>2)</sup>、[ $^{11}\text{C}$ ] SB-13<sup>3)</sup> の3つの PET 用プローブが探索的臨床研究に供されている。これらの中で最も進捗度の高いピッツバーグ大学の Klunk らによって開発された [ $^{11}\text{C}$ ] PIB について概説すると、AD 患者脳において高い集積の認め

用語解説—— $\beta$  シート構造

蛋白の高次構造の1つで、紙を蛇腹状に折りたたみ引き伸ばしたような状態。互いに隣接するペプチド鎖の NH 基と CO 基間で水素結合し、その結合が構造の安定化に寄与していると考えられている。

## Recommended Readings

- ① Neurobiol Aging 19 : No.2, 1998
- ② Klunk WE et al : Ann Neurol 55 : 306-319, 2004
- ③ Okamura N et al : J Neurosci 24 : 2535-2541, 2004

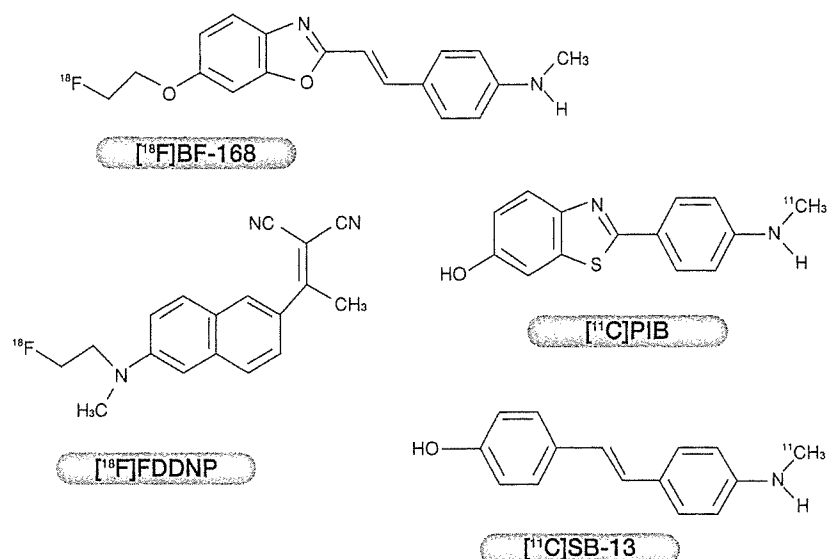


図 これまで報告されている代表的なアルツハイマー病診断用プローブ

られる部位は前頭葉，側頭頭頂葉などであるが，これらは明らかに健常コントロール画像と異なっており，また [<sup>18</sup>F] FDG 代謝の低下している部位に集積がみられた． [<sup>11</sup>C] PIB 集積の Standardized Uptake Value (SUV) と [<sup>18</sup>F] FDG の代謝率を比較したところ，前者の SUV のほうが後者の代謝率よりも AD 患者-健常コントロール間のデータのオーバーラップが少なかった．このことはこのプローブによる診断のほうが [<sup>18</sup>F] FDG を用いたそれよりも AD の診断精度が優れていることを示唆している．しかし一方，AD 患者において [<sup>11</sup>C] PIB 集積が正常レベルであった例，正常コントロールでも集積の高かった例などもみられている．これらが false positive/negative なのか，または発症前高リスク者であったのかは今後多例数を重ねて検討する必要がある．

[<sup>11</sup>C] SB-13<sup>3)</sup>は [<sup>11</sup>C] PIB とほとんど同じ成績であったことが報告されているが， [<sup>18</sup>F] FDDNP<sup>1)</sup>はかなり非特異的結合が多いことが知られている．

### わが国発のプローブ

日本においては筆者らによって開発された老人斑に選択性の高い BF-168<sup>4)</sup>のさらなる進化体である BF-227 (THK-002) と呼ばれるプローブの探索的臨床研究が，東北大学チームによって平成 17 年度から開始される予定である．

AD 診断のガイドライン的な役割を果たしているのが，いわゆるレーガン研究所の有名な Consensus Report<sup>5)</sup>である．同 Report が求めているのは，診断の感度および特異度はいずれも 80 % 以上，陽性的中率は 90 % である．これまでのプローブの感度などのデータはまだ報告されていないが，診断原理的にこれまでの診断法のそれらを凌ぐことが予想される．

アミロイドイメージングと，近年開発されつつあるワクチンなどの根本療法とを組み合わせることにより，診断時点で発症前でさえあれば AD に罹患せずに一生を送らせることを可能とする時代の足音が聞こえている．

#### References

- 1) Shoghi-Jadid K et al : Am J Geriatr Psychiatry 10 : 24-35, 2002
- 2) Klunk WE et al : Ann Neurol 55 : 306-319, 2004
- 3) Verhoeff NP et al : Am J Geriatr Psychiatry 12 : 584-595, 2004
- 4) Okamura N et al : J Neurosci 24 : 2535-2541, 2004
- 5) Neurobiol Aging 19 : No.2, 1998

#### 関連事項

- アルツハイマー型認知症(痴呆) ▶▶ 96 頁
- 老人斑 ▶▶ 212 頁
- βアミロイド前駆体蛋白(APP)とβアミロイド ▶▶ 216 頁
- PET ▶▶ 246 頁
- 診断マーカー ▶▶ 252 頁

ロウネン キ ニン チ ショウ

## 老年期認知症ナビゲーター

定価 本体4700円(税別)

2006年9月10日 第1版第1刷発行©

監修者 ヒライ ショウサク 平井俊策  
編集者 アラ イ ヒロユキ 荒井啓行 / ウラカミカツ ヤ 浦上克哉 / タケダ マサトシ 武田雅俊 / ホン マ アキラ 本間 昭  
発行者 松岡光明  
発行所 株式会社メディカルレビュー社

〒113-0034 東京都文京区湯島3-19-11 イトーピア湯島ビル  
電話/03-3835-3041(代)

編集部 電話/03-3835-3043 FAX/03-3835-3040  
✉ editor-1@m-review.co.jp

販売部 電話/03-3835-3049 FAX/03-3835-3075  
✉ sales@m-review.co.jp

〒541-0046 大阪市中央区平野町1-7-3 吉田ビル  
電話/06-6223-1468(代) 振替 大阪6-307302  
<http://www.m-review.co.jp>

印刷・製本／図書印刷株式会社  
用紙／株式会社松菱洋紙店

本書に掲載された著作物の複写・複製・転載・翻訳・データベースへの取り込みおよび送信(送信可能化権を含む)・上映・譲渡に関する許諾権は(株)メディカルレビュー社が保有しています。

**JICIS** <(株)日本著作出版権管理システム委託出版物>

本書の無断複写は著作権法上での例外を除き、禁じられています。複写される場合は、そのつど事前に(株)日本著作出版権管理システム(電話03-3817-5670)の許諾を得てください。

乱丁・落丁の際はお取り替えいたします。

ISBN 4-7792-0015-6 C3047

ORIGINAL ARTICLE

## Development of amyloid imaging PET probes for an early diagnosis of Alzheimer's disease

YUKITSUKA KUDO

Tohoku University Biomedical Engineering Research Organization (TUBERO), Sendai, Japan

### Abstract

Progressive accumulation of senile plaques (SPs) is one of the major neuropathological features of Alzheimer's Disease (AD) that precedes cognitive decline. Noninvasive detection of SPs could, therefore, be a potential diagnostic test for early or presymptomatic detection of AD patients. For this purpose, many attempts have been made to visualize AD-specific pathological changes in the living brain. Currently, a most practical method for the *in vivo* measurement of SP depositions is using positron emission tomography (PET) and contrast agent that specifically label SPs. We have developed a novel compound 2-[2-(2-dimethylaminothiazol-5-yl) ethenyl]-6-[2-(fluoro)ethoxy] benzoxazole (BF-227) as a candidate for an amyloid imaging probe for PET. BF-227 displayed high affinity to synthetic amyloid  $\beta$  fibrils and clearly stained both SPs and diffuse plaques in AD brain sections. Intravenous administration of [ $^{11}\text{C}$ ]BF-227 into normal mice indicated that this labeled tracer readily penetrated the blood brain barrier (BBB) and was washed out quickly from brain tissue. Currently, we have investigated the clinical trial of [ $^{11}\text{C}$ ]BF-227 in healthy subjects and AD patients.

**Key words:** Alzheimer's disease, early diagnosis, amyloid imaging probes, senile plaques, positron emission tomography

### Introduction

Alzheimer's disease (AD) is the most prevalent cause of dementia characterized by irreversible impairment of the cognitive function with accumulation of senile plaques (SPs) and neurofibrillary tangles (NFTs). It is well known that the pathological features in AD brains, especially accumulation of SPs, precede the clinical symptoms by more than a decade. These several lines of evidence indicate the existence of a temporally wide dissociation between the clinical and neuropathological features of AD. Direct imaging of SPs in patients with AD *in vivo* would be very useful for the early or presymptomatic diagnosis of AD.

For early diagnosis of AD, several imaging techniques have been developed that can noninvasively detect SPs in the brain using positron emission tomography (PET), single photon emission computed tomography (SPECT), and magnetic resonance imaging (MRI).

SPs are composed of the amyloid- $\beta$  protein ( $A\beta$ ), which is proteolytically cleaved from amyloid precursor proteins (1). NFTs, in contrast, are composed of phosphorylated tau(2). Many attempts have been made to visualize AD-specific pathological changes in the living brain. Currently, a most practical method for the *in vivo* measurement of SP depositions uses PET and a contrast agent that specifically labels SPs (3). The development of amyloid imaging agents starts with Congo-red and thioflavin-T, which have been commonly used for histochemical staining of amyloid. However, these agents lack some characteristics for suitable amyloid imaging probes as shown in Table I. In the past 10 years many candidate agents have been developed for amyloid imaging probes with different chemical structures and properties (Figure 1). A Congo-red derivative, Chrysamine-G was first introduced as a candidate for an *in vivo* probe of amyloid deposition (4). As a consequence of compound optimization, (trans, trans)-1-bromo-2,5-bis-(3-hydroxycarbonyl-1,4-hydroxy) styrylbenzene

Correspondence: Y. Kudo, Tohoku University Biomedical Engineering Research Organization (TUBERO), 2-1, Seiryomachi, Aoba-ku, Sendai, 980-8575, Japan. E-mail: kudoyk@tubero.tohoku.ac.jp

ISSN 1364-5706 print/ISSN 1365-2931 online © 2006 Taylor & Francis  
DOI: 10.1080/13645700600836000

Table I. Requirements for amyloid imaging probes for clinical application

- High binding affinity to amyloid- $\beta$  fibrils
- Selective binding to amyloid plaques
- High BBB permeability
- Fast clearance from normal brain tissue
- Metabolic stability
- Drug safety

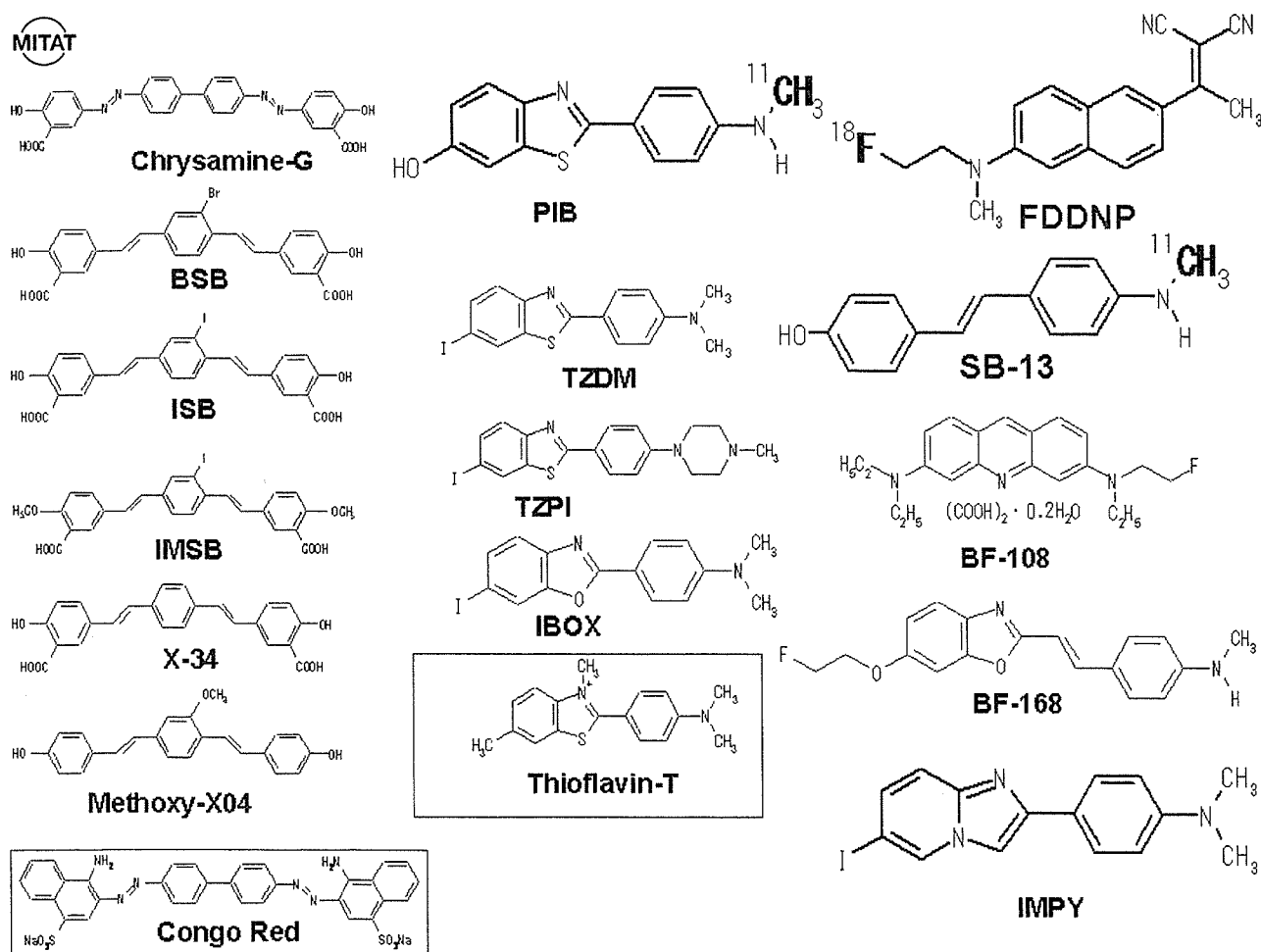
(BSB) and methoxy-X04 have successfully visualized the brain amyloid deposits of APP transgenic mice after intravenous administration of these compounds (5,6).

The first clinical amyloid imaging of the brain of AD patients used [ $^{18}\text{F}$ ] 2-(1-{ 6-[(2-fluoroethyl)-methyl-amino]-2-naphthyl } ethylidene) malononitrile ([ $^{18}\text{F}$ ]FDDNP) (7). The following second and third imaging used *N*-methyl-[ $^{11}\text{C}$ ]2-(4-methylaminophenyl)-6-hydroxybenzothiazole ([ $^{11}\text{C}$ ]PIB) and [ $^{11}\text{C}$ ]4-*N*-methylamino-4-hydroxystilbene ([ $^{11}\text{C}$ ]SB-13), respectively(8,9).

However, FDDNP has some weakness in practical use due to their considerable amount of nonspecific accumulation in normal brain tissue (10).

Compared with controls, AD patients typically showed marked retention of [ $^{11}\text{C}$ ]PIB in areas of association cortex known to contain large amounts of amyloid deposits in AD. In the AD patient group, PIB retention was increased most prominently in the frontal cortex. Large increases were also observed in parietal, temporal, and occipital cortices and the striatum. [ $^{11}\text{C}$ ]PIB retention was equivalent in AD patients and controls in areas known to be relatively unaffected by amyloid deposition (such as subcortical white matter, pons, and cerebellum) (8). The high retention of [ $^{11}\text{C}$ ]PIB in the frontal cortex conflicts with evidence from postmortem studies, in which the amyloid load is rarely highest in the frontal cortex (3).

Another amyloid imaging probe [ $^{11}\text{C}$ ]SB-13 was also applied in a human PET study and exhibited binding properties similar to [ $^{11}\text{C}$ ]PIB (9).

Figure 1. Chemical structures of imaging probes for *in vivo* detection of amyloid.

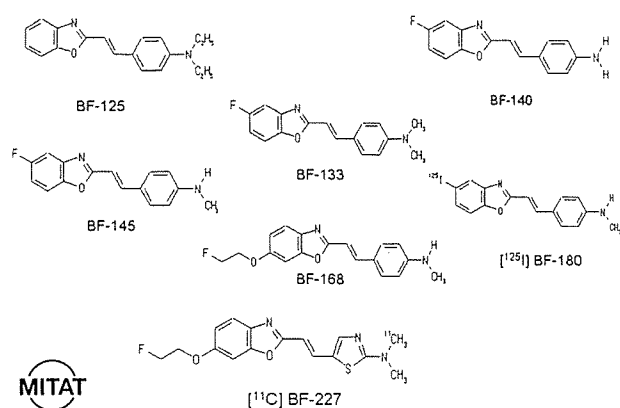


Figure 2. Chemical structures of our benzoxazole derivatives.

In Japan, our team has developed amyloid imaging probes since 1997 (Figure 2). We have previously reported a novel series of compounds including 6-(2-fluoroethoxy)-2-[2-(4-methylaminophenyl) ethenyl]-benzoxazole (BF-168), [2-(4-methylaminophenyl) ethenyl]-5-fluorobenzoxazole (BF-145) as promising candidates for *in vivo* imaging probes of SPs(11–13). These benzoxazole derivatives showed comparatively high permeability of blood-brain barrier (BBB), high affinity for A $\beta$  aggregates, and high specificity for amyloid plaques including diffuse plaques, which suggests potential merit for detection of AD-related pathology. However, for application of these derivatives in a clinical PET study, we need to optimize the pharmacokinetic and safety of these molecules, and introduce an optimized derivative 2-[2-(2-(2-dimethylaminothiazol-5-yl) ethenyl)-6-[2-(fluoro)ethoxy] benzoxazole (BF-227) as a candidate probe for *in vivo* imaging of amyloid in humans.

## Material and methods

### Affinity for synthetic A $\beta$ 1-42

Binding affinity of BF-227 for synthetic A $\beta$ 1-42 aggregates was examined as reported previously (12). Briefly, the binding assay was performed by mixing aliquot of aggregated A $\beta$ 1-42 with <sup>125</sup>I-labeled BF-180 (Figure 2).

### Neuropathological staining in AD brain section

Postmortem brain tissues from autopsy-conformed AD cases were obtained from Fukushi-mura Hospital (Toyohashi, Japan). Experiments were performed under regulations of the ethics committee of the BF Research Institute. Brain sections were immersed in 100  $\mu$ M of BF-227 solution containing 50 % ethanol.

### BBB permeability of [<sup>11</sup>C]BF-227 in normal mice

Brain uptakes of BF-227 were measured using <sup>11</sup>C-labeled compound. [<sup>11</sup>C]BF-227 was administered into the tail vein of normal mice. The mice were then sacrificed by decapitation at 2 and 60 min post injection (p.i.). The brains were removed and weighted, and the radioactivity was counted with an automatic  $\gamma$ -counter.

### Acute and subacute toxicity of BF-227

Non-GLP toxicity study was carried out using female and male mice.

### Other actions of BF-227

Postmortem brain section from autopsy-conformed AD cases was immersed in saline containing [<sup>11</sup>C]BF-227, dipped in water, washed with EtOH, dried, and an autoradiographic image of the dried section was obtained using BAS-5000 phosphorimaging system (Fujifilm, Japan).

*Ex vivo* plaque labeling with BF-227 was evaluated using PS1/APPsw double transgenic mice. A BF-227 solution was administered into the tail vein.

## Results

### Affinity for synthetic A $\beta$ 1-42

The K<sub>i</sub> value for A $\beta$ 1-42 fibrils in competitive binding assay using [<sup>125</sup>I]BF-180 was  $4.3 \pm 1.3$  nM in BF-227 (K<sub>d</sub> value of [<sup>125</sup>I]BF-180:  $10.8 \pm 1.5$  nM). This result suggests that BF-227 has a high binding affinity for A $\beta$ 1-42 fibrils.

### Neuropathological staining in AD brain section

BF-227 clearly stained many SPs and diffuse plaques. This staining pattern corresponded to that of A $\beta$  immunostaining in the adjacent section (Figure 3).

### BBB permeability of [<sup>11</sup>C]BF-227 in normal mice

Intravenous administration of [<sup>11</sup>C]BF-227 into normal mice indicated that this labeled tracer readily penetrated the BBB (7.9 %ID/g at 2 min p.i.) and was washed out quickly (0.64 %ID/g at 60 min p.i.) from brain tissue.

### Acute and subacute toxicity of BF-227

In an acute toxicity study, the lethal dose of BF-227 was larger than 10mg/kg (i.v.) for male and female

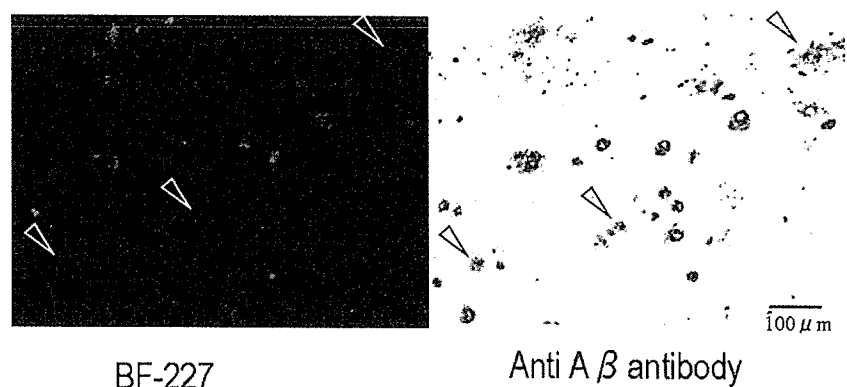


Figure 3. Neuropathological staining of amyloid plaques with BF-227 in AD brain sections. Sps and diffuse plaques (arrow head) were clearly stained with BF-227.

mice. In a subacute study, intravenous administration of BF-227 in tested doses did not produce any significant changes in general behavior and body weight. After 14 days post-treatment period, the mice did not show any microscopic alteration on pathological examination.

#### Other actions of BF-227

In the autoradiographic image using [ $^{11}\text{C}$ ]BF-227, a specific binding pattern in the AD brain section was observed in the grey matter including SPs.

In the brain sections of PS1/APP Tg mice after intravenous injection of BF-227, numerous fluorescent spots were observed in the neocortex and hippocampus of the brain. These fluorescent spots corresponded to those of A $\beta$  immunostaining in the same section.

#### Discussion and future prospects

BF-227 has high binding affinity to A $\beta$  fibrils, remarkable stainability for SPs, high permeability of BBB, and fast clearance from normal brain tissue. The toxicity study of BF-227 indicates the sufficient safety margin of this compound for PET probe. Currently, we have investigated the clinical trial of [ $^{11}\text{C}$ ]BF-227 in healthy subjects and in AD patients. This trial will elucidate the binding characteristics *in vivo* and the clinical usefulness of the probe in humans, and the results will be published by this summer or autumn.

Recently, we have introduced three novel compounds as candidate probes for *in vivo* imaging of tau pathology in the AD brain; 4-[2-(2-benzimidazolyl) ethenyl]-N, N-diethylbenzenamine (BF-126), 2-[(4-methylamino) phenyl] quinoline (BF-158), and 2-(4-aminophenyl) quinoline (BF-170) (14) (Figure 4). In neuropathological examination,

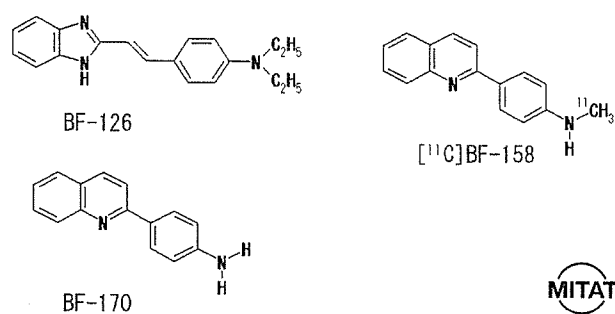


Figure 4. Chemical structures of our tau specific probes.

BF-126, BF-158, and BF-170 clearly stained NFTs, neuropil threads, and paired helical filament-type neuritis in the AD brain section. In addition, NFTs was labeled by  $^{11}\text{C}$ -labeled BF-158 with autoradiography. These findings suggest the potential usefulness of quinoline and benzimidazole derivatives for *in vivo* imaging of tau pathology in AD.

Several  $^{11}\text{C}$  labeled probes for detecting SPs in AD patients have been reported from some teams. The short half-life (20 min) of  $^{11}\text{C}$ , however, may limit the usefulness of these probes for a widespread application. Comparable  $^{18}\text{F}$  labeled probes may supplant the clinical need due to the longer half-life of the isotope (109.7 min) (15). Further studies to develop  $^{18}\text{F}$  labeled PET probes for the imaging of SPs are currently under way in some teams, including ours.

Unlike Alois Alzheimer, we now have access to instrumentation that allows visualization of the human brain *in vivo*. Brain imaging has become a part of the routine clinical assessment of dementia disorder (16). Recently, anti-amyloid agents such as A $\beta$  vaccine and selective secretase inhibitors have been developed for the causal therapy of AD patients. AD patients all over the world may be

effectively diagnosed and treated by a combination of presymptomatic diagnosis and causal therapy.

### Acknowledgement

The author thanks all the present and past members of our team and collaborators.

This study was financially supported by the Special Coordination Funds for Promoting Science and Technology, the Health and Labour Sciences Research Grants for Translational research from Ministry of Health, Labour and Welfare, Japan, the Program for Promotion of Fundamental Studies in Health Science of the National Institute of Biomedical Innovation, the New Energy and Industrial Technology Development Organization (NEDO), the Novartis foundation for Gerontological Research, the AstraZeneca Research Grant, and the Mitsui Sumitomo Insurance Welfare.

### References

1. Shoji M, Golde TE, Ghiso J, Cheung TT, et al. Production of the Alzheimer amyloid beta protein by normal proteolytic processing. *Science*. 1992;258:126–9.
2. Lee VM, Balin BJ, Otvos L, Jr. Trojanowski JQ. A68: a major subunit of paired helical filaments and derivatized forms of normal Tau. *Science*. 1991;251:675–8.
3. Nordberg A. PET imaging of amyloid in Alzheimer's disease. *Lancet Neurol*. 2004;3:519–27.
4. Klunk WE, Debnath ML, Pettegrew JW. Chrysamine-G binding to Alzheimer and control brain: autopsy study of a new amyloid probe. *Neurobiol Aging*. 1995;16:541–8.
5. Skovronsky DM, Zhang B, Kung MP, Kung HF, et al. In vivo detection of amyloid plaques in a mouse model of Alzheimer's disease. *Proc Natl Acad Sci U S A*. 2000;97:7609–14.
6. Klunk WE, Bacskai BJ, Mathis CA, Kajdasz ST, et al. Imaging Abeta plaques in living transgenic mice with multi-photon microscopy and methoxy-X04, a systemically administered Congo red derivative. *J Neuropathol Exp Neurol*. 2002;61:797–805.
7. Shoghi-Jadid K, Small GW, Agdeppa ED, Kepe V, et al. Localization of neurofibrillary tangles and beta-amyloid plaques in the brains of living patients with Alzheimer disease. *Am J Geriatr Psychiatry*. 2002;10:24–35.
8. Klunk WE, Engler H, Nordberg A, Wang Y, et al. Imaging brain amyloid in Alzheimer's disease with Pittsburgh Compound-B. *Ann Neurol*. 2004;55:306–19.
9. Verhoeff NP, Wilson AA, Takeshita S, Trop L, et al. In-vivo imaging of Alzheimer disease beta-amyloid with [11C]SB-13 PET. *Am J Geriatr Psychiatry*. 2004;12:584–95.
10. Bacskai BJ, Klunk WE, Mathis CA, Hyman BT. Imaging amyloid-beta deposits in vivo. *J Cereb Blood Flow Metab*. 2002;22:1035–41.
11. Okamura N, Suemoto T, Shiomitsu T, Suzuki M, et al. A novel imaging probe for in vivo detection of neuritic and diffuse amyloid plaques in the brain. *J Mol Neurosci*. 2004;24:247–55.
12. Okamura N, Suemoto T, Shimadzu H, Suzuki M, et al. Styrylbenzoxazole derivatives for in vivo imaging of amyloid plaques in the brain. *J Neurosci*. 2004;24:2535–41.
13. Shimadzu H, Suemoto T, Suzuki M, Shiomitsu T, et al. Novel probes for imaging amyloid-beta: F-18 and C-11 labeling of 2-(4-aminostyryl)benzoxazole derivatives. *Journal of Labelled Compounds & Radiopharmaceuticals*. 2004;47:181–90.
14. Okamura N, Suemoto T, Furumoto S, Suzuki M, et al. Quinoline and benzimidazole derivatives: candidate probes for in vivo imaging of tau pathology in Alzheimer's disease. *J Neurosci*. 2005;25:10857–62.
15. Chandra R, Kung MP, Kung HF. Design, synthesis, and structure-activity relationship of novel thiophene derivatives for beta-amyloid plaque imaging. *Bioorg Med Chem Lett*. 2006;16:1350–2.
16. Nordberg A. Is amyloid plaque imaging the key to monitoring brain pathology of Alzheimer's disease in vivo? *Eur J Nucl Med Mol Imaging*. 2004;31:1540–3.



## Styrylbenzazole derivatives for imaging of prion plaques and treatment of transmissible spongiform encephalopathies

Kensuke Ishikawa,\* Yukitsuka Kudo,† Noriyuki Nishida,‡ Takahiro Suemoto,§ Tohru Sawada,§ Toru Iwaki¶ and Katsumi Doh-ura\*

\*Department of Prion Research, Tohoku University Graduate School of Medicine, Sendai, Japan

†Division of Telecommunication and Information Technology, Biomedical Engineering Research Organization, Tohoku University, Sendai, Japan

‡Division of Cellular and Molecular Biology, Nagasaki University Graduate School of Biomedical Sciences, Nagasaki, Japan

§BF Research Institute Inc., Osaka, Japan

¶Department of Neuropathology, Graduate School of Medical Sciences, Kyushu University, Fukuoka, Japan

### Abstract

Recent prevalence of acquired forms of transmissible spongiform encephalopathies (TSEs) has urged the development of early diagnostic measures as well as therapeutic interventions. To extend our previous findings on the value of amyloid imaging probes for these purposes, styrylbenzazole derivatives with better permeability of blood–brain barrier (BBB) were developed and analyzed in this study. The new styrylbenzazole compounds clearly labeled prion protein (PrP) plaques in brain specimens from human TSE in a manner irrespective of pathogen strain, and a representative compound BF-168 detected abnormal PrP aggregates in the brain of TSE-infected mice when the probe was injected intravenously. On the other hand, most of the compounds inhibited abnormal PrP

formation in TSE-infected cells with  $IC_{50}$  values in the nanomolar range, indicating that they represent one of the most potent classes of inhibitor ever reported. BF-168 prolonged the lives of mice infected intracerebrally with TSE when the compound was given intravenously at the preclinical stage. The new compounds, however, failed to detect synaptic PrP deposition and to show pathogen-independent therapeutic efficacy, similar to the amyloid imaging probes we previously reported. The compounds were BBB permeable and non-toxic at doses for imaging and treatment; therefore, they are expected to be of practical use in human TSE.

**Keywords:** amyloid imaging, anti-prion activity, pathogen strain, prion disease, styrylbenzazole derivatives.

*J. Neurochem.* (2006) **99**, 198–205.

The transmissible spongiform encephalopathies (TSEs) or prion diseases form a group of neurodegenerative disorders characterized by abnormal deposition of protease-resistant isoforms of prion protein (PrP) in the CNS (Prusiner 1991). TSEs are classified as sporadic, hereditary or environmentally acquired, and have become a serious public health issue because of the recent prevalence of acquired Creutzfeldt–Jakob disease (CJD), such as the variant form due to bovine spongiform encephalopathy (Will *et al.* 1996) and the iatrogenic form with cadaveric growth hormone or dura grafts (Brown *et al.* 2000). There is an urgent need to develop prophylactic and therapeutic interventions as well as diagnostic measures at the preclinical or early clinical stages of these incurable diseases.

We have previously reported that some amyloid imaging compounds, primarily derived from amyloid dyes such as

Received February 16, 2006; revised manuscript received May 25, 2006; accepted May 30, 2006.

Address correspondence and reprint requests to Dr Kensuke Ishikawa, Division of Prion Biology, Department of Prion Research, Tohoku University Graduate School of Medicine, 2–1 Seiryomachi, Aoba-ku, Sendai 980-8575, Japan. E-mail: ishikawa@mail.tains.tohoku.ac.jp

**Abbreviations used:** AD, Alzheimer's disease; BBB, blood–brain barrier; BSB, (trans, trans)-1-bromo-2,5-bis-(3-hydroxycarbonyl-4-hydroxy)styrylbenzene; CJD, Creutzfeldt–Jakob disease; DMSO, dimethylsulfoxide; FDDNP, 2-(1-[6-[(2-fluoroethyl)(methyl)amino]-2-naphthyl]ethylidene)malononitrile; GSS, Gerstmann–Sträussler–Scheinker syndrome; ICR, Institute of Cancer Research; ID, injected dose; NT, not tested; PrP, prion protein; PrPres, protease-resistant PrP; PTA, phosphotungstic acid; PVDF, polyvinylidene difluoride; TSE, transmissible spongiform encephalopathy.

Congo red and thioflavin T, are useful for detection of prion plaques and treatment of TSE (Ishikawa *et al.* 2004). These compounds, however, are limited in their ability because of inefficient brain uptake. Here we describe new compounds, styrylbenzazole derivatives, which have been developed for practical use and analyzed for their PrP imaging ability, anti-prion activity, therapeutic efficacy, brain uptake and toxicity.

## Materials and methods

### Chemicals and experimental models

All of the test compounds were synthesized at Tanabe R & D (Saitama, Japan) and used freshly after being dissolved in 100% dimethylsulfoxide (DMSO).

Cultured cells were grown in Opti-MEM (Invitrogen, Carlsbad, CA, USA) supplemented with 10% fetal calf serum. As cellular models of TSE, we used mouse neuroblastoma (N2a) cells persistently infected with the RML strain (ScN2a) (Race *et al.* 1988) and six other prion-infected cell lines: N2a58 cells individually infected with the RML strain, the 22L strain (Nishida *et al.* 2000) and Fukuoka-1 strain (Ishikawa *et al.* 2004); N2a cells infected with the 22L strain; mouse hypothalamic cells (GT1-7) infected with the 22L strain (Milhavet *et al.* 2000); and mouse fibroblast cells (L929) infected with the RML strain (Vorberg *et al.* 2004).

Tg7 mice overexpressing hamster PrP (Race *et al.* 1995) and Tga20 mice overexpressing mouse PrP (Fischer *et al.* 1996) were also used. These mouse models were intracerebrally infected with 20  $\mu$ L brain homogenate comprising 1% (w/v) of the 263K strain and the RML strain respectively. The Tg7 mice showed plaque-type PrP deposition between the cerebral cortex and hippocampus by 6 weeks after infection, followed by synaptic-type PrP deposition in the thalamus. The Tga20 mice showed similar pathological deposition, but plaques were not seen as frequently. Each mouse weighed ~30 g, and was maintained under deep ether anesthesia for minimum distress during all surgical procedures. Permission for the animal study was obtained from either the Animal Experiment Committee of Kyushu University or Tohoku University, Japan.

### Brain uptake study

Test compounds were administered intravenously to Institute of Cancer Research (ICR) mice under ether anesthesia to determine initial brain uptakes. At 2 or 30 min after injection, the brains were removed, weighed and homogenized with saline. After centrifugation of the homogenate at 21 900 g for 10 min, the supernatant was applied to a conditioned C18 solid-phase extraction cartridge, and the compounds were eluted with methyl alcohol. Fluorescence was detected by high performance liquid chromatography with a fluorescence detector as reported previously (Okamura *et al.* 2005), and the percentage of injected dose per gram (%ID/g) was used as a measure of the level of the compounds in the brain.

### *In vitro* PrP imaging in sections

Autopsy-diagnosed brain samples from cases of Gerstmann-Sträussler-Scheinker syndrome (GSS) ( $n = 2$ ), sporadic CJD ( $n = 5$ ), iatrogenic dura CJD with synaptic PrP deposition ( $n = 1$ ) and non-TSE control cases with amyloid lesions [Alzheimer's disease (AD),  $n = 2$ ] or without amyloid lesions (cerebral infarction,  $n = 1$ )

were obtained from the Department of Neuropathology, Kyushu University, Japan. After fixation in 10% buffered formalin for 2 weeks, each sample of TSE was immersed in 98% formic acid for the reduction of prion infectivity, embedded in paraffin and cut into sections 7  $\mu$ m thick. Sections of a variant CJD case were kindly provided by Dr James W. Ironside of the CJD Surveillance Unit, Edinburgh, UK. For neuropathological staining, deparaffinized sections were immersed in 1% Sudan black solution to quench tissue autofluorescence. They were then incubated for 30 min in 1- $\mu$ M solutions of the test compounds, rinsed with distilled water and examined under a fluorescence microscope (DMRXA; Leica Instruments, Wetzlar, Germany) with a UV or FITC filter set.

For comparison, each section was subsequently immunoassayed for PrP as described previously (Doh-ura *et al.* 2000). Briefly, the sections were treated with a hydrolytic autoclave and incubated with a rabbit primary antibody, c-PrP, which was raised against a mouse PrP fragment, amino acids 214–228 (1 : 200; Immuno-Biological Laboratories, Gunma, Japan), followed by incubation with a horseradish peroxidase-conjugated secondary antibody (1 : 200; Vector Laboratories, Burlingame, CA, USA). The reaction product was developed with 3,3'-diaminobenzidine tetrahydrochloride solution and counterstained with hematoxylin. Paraffin-embedded brains of experimental animals were similarly investigated.

### *In vivo* PrP imaging in model animals

BF-168 (molecular weight 312.34) dissolved in 10% DMSO was administered intravenously (0.5–5 mg/kg body weight) into Tg7 mice at 6–7 weeks after injection when the mice showed no apparent clinical signs of TSE. As controls, vehicle alone was similarly injected into infected mice, and BF-168 was administered into uninfected mice. The animals were killed at various time points, and the brains were rapidly frozen and cut into coronal sections 10  $\mu$ m thick using a cryostat (CM3050; Leica Instruments). The sections were thaw-mounted on slides, dried and coverslipped. They were examined under a fluorescence microscope and further analyzed immunohistochemically as described above.

### *In vitro* treatment in cell cultures

Abnormal PrP formation was assayed by the content of protease-resistant PrP (PrPres) in cellular models of TSE as described previously (Caughy and Raymond 1993). Each compound was added at the designated concentrations when cells were passaged at 10% confluence, while maintaining the final concentration of DMSO in the medium at < 0.5%. The cells were allowed to grow to confluence and lysed with lysis buffer (0.5% sodium deoxycholate, 0.5% Nonidet P-40, phosphate-buffered saline). For analysis of PrPres, samples were digested with 10  $\mu$ g/mL proteinase K for 30 min, and the digestion was stopped with 0.5 mM phenylmethylsulfonyl fluoride. The samples were centrifuged at 100 000 g for 30 min, and pellets were resuspended in 1  $\times$  sample loading buffer and boiled. For analysis of cellular PrP in N2a cells, cell lysates were mixed directly with a quarter volume of 5  $\times$  sample loading buffer and boiled. These samples were separated by electrophoresis on a 15% Tris-glycine-sodium dodecyl sulfate polyacrylamide gel and electroblotted on to a polyvinylidene difluoride (PVDF) filter (Millipore, Bedford, MA, USA). PrP was detected using a monoclonal antibody, SAF83 (1 : 5000; SPI-BIO, Massy, France), followed by an alkaline phosphatase-conjugated

goat anti-mouse antibody (1 : 20 000; Promega, Madison, WI, USA). Immunoreactive blots were visualized with CDP-Star detection reagent (Amersham, Piscataway, NJ, USA). More than two independent assays were performed in each experiment and signals were analyzed using image analysis software. The approximate concentration of the compound giving 50% inhibition of PrPres formation, relative to the vehicle-treated control ( $IC_{50}$ ), was estimated by signal intensity. To control for the detection limits of western blotting, we performed additional experiments utilizing sodium phosphotungstic acid (PTA) precipitation, which is the most sensitive technique presently available to detect PrPres (Safar *et al.* 1998). The PTA precipitation was undertaken on cell lysates of ScN2a treated with BF-168 at a designated concentration. The resulting pellets were collected by centrifugation and then analyzed by immunoblotting as described above.

#### *In vivo* treatment in model animals

BF-168 solution (4 mg/kg body weight) or vehicle alone was injected intravenously to experimental animals ( $n = 5$ ) once a week. The treatment was started at 2 weeks after injection for Tg7 mice and at 4 weeks after injection for Tga20 mice, and repeated for 4 weeks. A continuous subcutaneous infusion of BF-168 was also given to Tga20 mice ( $n = 5$ ) using an Alzet osmotic pump (Durect, Cupertino, CA, USA). In accordance with the manufacturer's instructions, each pump was filled with BF-168 solution at the designated doses and placed in a subcutaneous area of the back at 4 weeks after injection. The animals showed no apparent adverse effects of the treatment and were monitored 5 days a week until obvious clinical signs appeared. Statistical significance was analyzed by one-way ANOVA followed by Scheffé's method for multiple comparisons.

## Results

### Brain uptake and toxicity

We designed and synthesized novel styrylbenzoxazole derivatives (Table 1), styrylbenzothiazole and styrylbenzimidazole derivatives (Table 2) with more efficient permeability of the BBB and less toxicity. Values for brain uptake at 2 min after intravenous injection of the compounds were in the 2.4–17.0%ID/g range, indicating a satisfactory level for imaging probes. Their washouts from the brain varied, with the ratio of %ID/g at 2 min to that at 30 min after injection ranging from 1.0 to 56.9. Acute toxicity was tested by administering each compound intravenously at ~10 mg/kg body weight into normal ICR mice. No apparent toxic effect was observed with any of the compounds tested.

### PrP imaging ability

Imaging of abnormal PrP deposition by the compounds was first performed in brain sections of human TSE. The compounds fluorescently labeled most of the PrP plaques in cerebellar cortices of both GSS cases (Fig. 1a, representative data). Among sections from the sporadic CJD cases, PrP deposition was labeled only in a case with plaques (Fig. 1c). In the cerebral cortex from the variant CJD case, large core plaques were detectable, whereas the majority of immunopositive aggregates were not labeled (Fig. 1e). In contrast, no fluorescence signal was identified in sections from the dura CJD case or the other sporadic CJD cases that

**Table 1** Chemical structure, PrPres inhibition and brain uptake of styrylbenzoxazole derivatives including BF-168

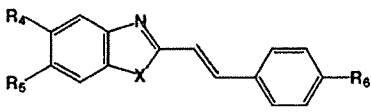
Compound	R <sub>1</sub>	R <sub>2</sub>	R <sub>3</sub>	IC <sub>50</sub> (nM) <sup>a</sup>	Brain uptake (%ID/g) <sup>b</sup>		Ratio of 2 to 30 min brain uptake
					2 min	30 min	
BF-168	H	O(CH <sub>2</sub> ) <sub>2</sub> F	NH(CH <sub>3</sub> )	0.4	3.9 <sup>c</sup>	1.6	2.4
BF-125	H	H	N(C <sub>2</sub> H <sub>5</sub> ) <sub>2</sub>	10.2	3.0	3.0	1.0
BF-133	F	H	N(CH <sub>3</sub> ) <sub>2</sub>	1.6	5.5	3.8	1.4
BF-135	NO <sub>2</sub>	H	N(CH <sub>3</sub> ) <sub>2</sub>	< 1	NT <sup>d</sup>	NT	-
BF-140	F	H	NH <sub>2</sub>	< 1	5.5	1.1	5.0
BF-145	F	H	NH(CH <sub>3</sub> )	< 1	4.4	1.6	2.8
BF-148	H	F	N(CH <sub>3</sub> ) <sub>2</sub>	< 1	NT	NT	-
BF-165	H	H	NH(CH <sub>3</sub> )	7.1	7.2	NT	-
BF-169	H	OH	NH(CH <sub>3</sub> )	2.4	NT	NT	-
BF-173	I	H	NH <sub>2</sub>	2.2	NT	NT	-
BF-180	I	H	NH(CH <sub>3</sub> )	8.5	2.4	1.8	1.3
BF-191	H	H	Cl	1.8	12.0	1.7	7.1
BF-208	H	H	F	< 1	11.0	0.53	20.8
N-282	H	H	N(CH <sub>3</sub> ) <sub>2</sub>	2.1	4.0	1.7	2.4
N-407	H	H	H	< 1	17.0	0.99	17.2

<sup>a</sup>IC<sub>50</sub>, approximate concentration of a compound giving 50% inhibition of PrPres formation relative to the control in ScN2a cells.

<sup>b</sup>%ID/g, percentage of injected dose per gram in the brains of normal mice.

<sup>c</sup>already reported in the previous work (Okamura *et al.*, 2004).

<sup>d</sup>NT, not tested.

**Table 2** Chemical structure, PrPres inhibition and brain uptake of styrylbenzothiazole and styrylbenzimidazole derivatives


Compound	X	R <sub>4</sub>	R <sub>5</sub>	R <sub>6</sub>	IC <sub>50</sub> (nM) <sup>a</sup>	Brain uptake (%ID/g) <sup>b</sup>		Ratio of 2 to 30min brain uptake
						2 min	30 min	
BF-124	S	H	H	N(C <sub>2</sub> H <sub>5</sub> ) <sub>2</sub>	18.1	2.4	2.5	1.0
BF-162	S	F	H	N(CH <sub>3</sub> ) <sub>2</sub>	1.4	NT <sup>c</sup>	NT	-
N-276	S	H	H	N(CH <sub>3</sub> ) <sub>2</sub>	< 1	NT	NT	-
N-438	S	H	H	H	< 1	11.0	2.0	5.5
BF-126	NH	H	H	N(C <sub>2</sub> H <sub>5</sub> ) <sub>2</sub>	21	7.2	0.16	45
BF-166	NH	F	H	N(C <sub>2</sub> H <sub>5</sub> ) <sub>2</sub>	1.1	NT	NT	-
N-457	NH	H	H	Cl	< 1	7.1	0.21	33.8
N-491	NH	H	H	H	1.9	7.4	0.13	56.9

<sup>a</sup>IC<sub>50</sub>, approximate concentration of a compound giving 50% inhibition of PrPres formation relative to the control in ScN2a cells.

<sup>b</sup>%ID/g, percentage of injected dose per gram in the brains of normal mice.

<sup>c</sup>NT, not tested.

included perivacuolar and/or synaptic PrP deposition (data not shown). Background staining was barely observed after rinsing off the excess compound. Immunohistochemical analysis of PrP revealed that the compounds achieved high-specificity labeling (Figs 1b, d and f). The compounds displayed no signal in control sections without amyloid lesions (data not shown).

Similar results were observed in experimental mice. PrP plaques were specifically labeled in brain sections of Tg7 mice infected with the 263K strain, and there was no PrP immunopositive reaction or fluorescence signal in brain sections of uninfected mice (data not shown). We performed *in vivo* experiments using presymptomatic Tg7 mice at a later stage of TSE. A typical image is shown in Fig. 1(g); peripheral administration of BF-168 fluorescently labeled plaques in the cerebral white matter, indicating that the compound efficiently entered the brain and bound to coarse PrP deposits. Subsequent immunostaining verified the specificity and sensitivity for PrP (Fig. 1h). Non-specific staining, such as cerebrovascular labeling, was occasionally observed at 4 h after injection of 5 mg/kg BF-168, but not after 8 h or more. The stability of the fluorescence signals was examined at various time points up to 24 h after injection and the dye-PrP complex remained visible at the latest time. In contrast, there was no significant labeling after an injection of BF-168 into uninfected animals, or after an injection of vehicle alone to terminally ill Tg7 mice. Similar results were obtained for Tga20 mice infected with the RML strain, although plaques were less frequently detected (data not shown).

#### Anti-prion activity *in vitro*

The anti-prion activities of the compounds were investigated using ScN2a cells, which are most commonly used for drug screening for TSE treatment. Styrylbenzothiazole derivatives,

including BF-168, were evaluated and confirmed to inhibit PrPres formation with IC<sub>50</sub> values in the nanomolar or subnanomolar range (Fig. 2a and Table 1). Styrylbenzothiazole and styrylbenzimidazole derivatives were similarly potent, in a dose-dependent manner, within a non-toxic dose range (~10 μM) (Table 2). Treatment with vehicle alone showed no inhibitory effect compared with untreated controls (Fig. 2a). We utilized PTA precipitation, which increases the sensitivity of western blotting, and confirmed the potency of BF-168 at a concentration of 10 times the IC<sub>50</sub>. Furthermore, radiographic film was exposed to the blotted PVDF membranes for 10 times longer than usual before developing. No significant signals were visualized, whereas bands representing the vehicle-treated control were so strong as to be already saturated (Fig. 2b). To determine whether the efficacy was transient, ScN2a cells treated with 10 nM BF-168 were further cultured for 2 weeks in the absence of BF-168. PrPres signals never reappeared, even through four passages after discontinuation of the treatment (Fig. 2c). To exclude the possibility of interference with immunodetection, BF-168 solution at a final concentration of 10 nM was added to a lysate of untreated ScN2a cells before proteinase K digestion. PrP signals were not affected (data not shown). Nor was any alteration observed in cellular PrP level of N2a cells after treatment with 10 nM BF-168 (Fig. 2d).

To investigate whether the efficacy of the compounds depends on pathogen strain, we tested BF-168 in three N2a58 cell lines individually infected with different strains. As shown in Table 3, BF-168 was only effective in N2a58 cells infected with the RML strain, although the inhibitory activity was not as strong as in ScN2a cells (~1 μM). In contrast, BF-168 was ineffective in the same N2a58 cells infected with the 22L or Fukuoka-1 strains up to 10 μM, a dose at which the compound showed host cytotoxicity.